

Chiral loops and ghost states in the quenched scalar propagator

W. Bardeen,¹ A. Duncan,² E. Eichten,¹ N. Isgur,³ and H. Thacker⁴

¹Fermilab, P.O. Box 500, Batavia, Illinois 60510

²Department of Physics and Astronomy, University of Pittsburgh, Pittsburgh, Pennsylvania 15260

³Jefferson Lab, 12000 Jefferson Avenue, Newport News, Virginia 23606

⁴Department of Physics, University of Virginia, Charlottesville, Virginia 22901

(Received 15 June 2001; published 11 December 2001)

The scalar, isovector meson propagator is analyzed in quenched QCD, using the modified quenched approximation pole-shifting ansatz to study the chiral limit. In addition to the expected short-range exponential falloff characteristic of a heavy scalar meson, the propagator also exhibits a longer-range, negative metric contribution which becomes pronounced for smaller quark masses. We show that this is a quenched chiral loop effect associated with the anomalous structure of the η' propagator in quenched QCD. Both the time dependence and the quark mass dependence of this effect are well described by a chiral loop diagram corresponding to an η' - π intermediate state, which is light and effectively of negative norm in the quenched approximation. The relevant parameters of the effective Lagrangian describing the scalar sector of the quenched theory are determined.

DOI: 10.1103/PhysRevD.65.014509

PACS number(s): 12.38.Gc, 11.15.Ha, 11.30.Rd, 12.39.Fe

I. INTRODUCTION

For the foreseeable future, the quenched approximation will continue to play an important role in the study of lattice QCD for both practical and theoretical reasons. The practical reasons are only too obvious, considering the orders-of-magnitude increase in computer resources required for comparable full QCD simulations. But quenched QCD also provides a very instructive counterpoint to the full theory which can yield useful insight into the effect of quark loops in determining hadron structure. This is particularly true in the light-quark limit, where lattice results can be interpreted theoretically with the aid of an effective field theory corresponding to quenched chiral perturbation theory.

The introduction of quenched chiral perturbation theory by Sharpe, Bernard, and Golterman [1,2] established the framework for analyzing the chiral behavior of quenched QCD. This work focused attention on the particular, anomalous role of the quenched η' propagator. The physical η' is approximately a flavor singlet and gets most of its mass from the axial anomaly via repeated $q\bar{q}$ annihilation. In the quenched approximation, a single annihilation vertex can appear if both sides of the “hairpin diagram” are attached to valence quark lines, but repeated annihilation cannot take place without the closed quark loops of the unquenched theory. Instead of canceling the Goldstone pole in the valence quark (“connected”) diagram, the single annihilation diagram contributes a term to the η' propagator which has a *double* Goldstone pole and an overall sign opposite to that of the valence diagram. Unlike full QCD where η' loops remain infrared finite in the chiral limit, in the quenched theory, the double Goldstone pole of the hairpin term produces additional quenched chiral loop (QCL) singularities which alter the chiral behavior of the theory. This QCL effect was first observed in lattice results as a deviation from linear behavior of the squared pion mass as a function of quark mass [3,4]. Recently, the quenched chiral limit was extensively investigated in a high-statistics study at $\beta=5.7$ [5].

The problem of exceptional configurations, which had prevented previous studies from probing the smaller quark mass region of $m_\pi < 350$ MeV, was resolved by the pole-shifting ansatz of the modified quenched approximation (MQA) [6]. The QCL effect was observed in both the pseudoscalar mass and decay constants at the level expected from a direct study of the η' -hairpin mass insertion and the topological susceptibility. This established several independent and quantitatively consistent determinations of the quenched chiral log coefficient parameter δ (or, equivalently, of the η' mass insertion m_0^2).

The spectroscopy of scalar mesons has long been one of the murkier areas of hadron phenomenology. The well-established scalar mesons are typically at masses of a GeV or more, although there have been occasional, fleeting experimental indications of lower mass scalar resonances. In the flavor singlet sector, mixing with glueball states further complicates the interpretation of experimental data. This is clearly an area where lattice QCD calculations can be expected to play a crucial role in the future. High-statistics quenched studies will undoubtedly be an important part of this effort. Naively, we might expect that the anomalous chiral behavior induced by the quenched approximation would be of little importance for scalar-meson spectroscopy, since the meson masses involved are all expected to be quite heavy and not particularly sensitive to the details of chiral extrapolation. However, as we show in this paper, a more careful theoretical analysis combined with a precise numerical study of the scalar, isovector meson propagator at very light-quark mass reveals perhaps the most striking quenched chiral loop effect yet observed.

The chiral loop effect we discuss here is exhibited very clearly by comparing the scalar, isovector propagator for the heaviest- and lightest-quark masses studied. These are shown in Fig. 1. For the heaviest-quark mass the propagator is a positive and rapidly falling exponential, as expected from heavy scalar-meson intermediate states. The fit shown is a sum of two exponentials with the excited-state a_0^* mass extracted by comparing local-local, smeared-local, and

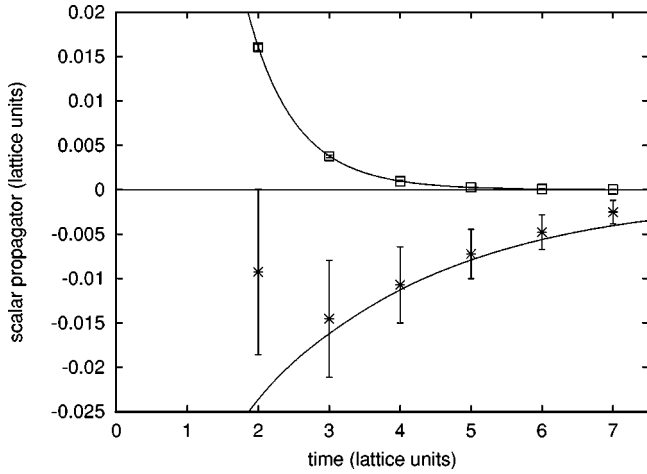


FIG. 1. The scalar propagator for the heaviest- ($\kappa = .1400$) and lightest- ($\kappa = .1428$) quark masses studied. For heavy quarks (boxes) the propagator is positive and exponentially falling. The (upper) solid curve is a two-exponential fit. For light quarks (*'s) the propagator exhibits a negative quenched chiral loop effect. The lower solid curve is the prediction of one-loop chiral perturbation theory for this term. (See Sec. II.)

smear-d-smeared correlators. (See the discussion in Sec. III.) By contrast, the scalar propagator for lighter quarks exhibits a qualitatively different behavior. (The lower curve in Fig. 1 is the one-loop quenched χPT prediction for the contribution to the scalar propagator of the $\eta' - \pi$ intermediate state only. See below and Sec. II.) This unusual behavior has two qualitative features which point clearly to a specific theoretical interpretation: (1) The additional component becomes much more prominent for the lightest-quark masses, and (2) the sign of this component is negative (i.e., opposite to that required by positivity of the spectral function). Both of these properties suggest that the new component is an effect of the $\eta' - \pi$ intermediate state, which is light in the quenched approximation. This contribution arises from the “hairpin + pion” diagram shown in Fig. 2(b). This interpretation also

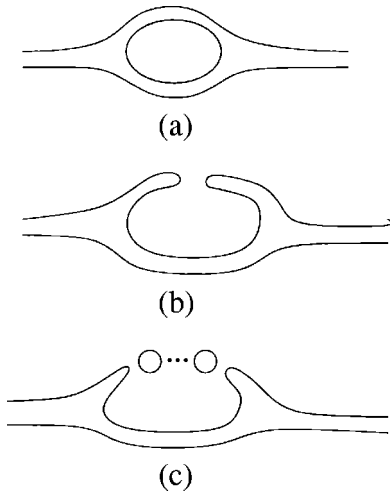


FIG. 2. Quark-line diagrams which contribute to the $\eta' - \pi$ intermediate state in the scalar isovector propagator.

TABLE I. Fit parameters for the scalar propagator, with m_0 fixed. The fit range is $t = [1 - 6]$.

κ	m_p	f_s	m_s	χ^2/dof
.1400	.603(2)	.0544(10)	1.20(2)	1.7/4
.1405	.556(2)	.0548(10)	1.19(2)	2.0/4
.1410	.505(2)	.0550(11)	1.17(2)	1.9/4
.1415	.450(3)	.0554(12)	1.16(3)	1.7/4
.1420	.386(3)	.0559(14)	1.16(4)	1.7/4
.1423	.342(4)	.0565(19)	1.18(5)	2.3/4
.1425	.307(4)	.0569(25)	1.19(7)	3.7/4
.1427	.267(5)	.0568(38)	1.20(12)	5.6/4
.1428	.245(6)	.0571(54)	1.29(18)	6.2/4

explains the fact that this component has a negative spectral weight. The hairpin (single mass insertion) diagram appears in the η' propagator with the opposite sign from that of the full propagator. In full QCD the $\eta' - \pi$ intermediate state would arise from three different types of quark-line diagrams: Fig. 2(a) with a single vacuum loop going around the entire diagram: Fig. 2(b) with a single hairpin vertex, and the type of graphs in Fig. 2(c) with one or more vacuum bubbles inserted into the η' propagator. Of these three, only the hairpin diagram, Fig. 2(b), is included in the quenched approximation. Since the single hairpin insertion has an overall negative sign (corresponding to a positive η' mass shift), the sign of this contribution is opposite to that which would be required by spectral positivity. The prominence of this negative term in our measured propagator is a clear example of the unitarity violation induced by the quenched approximation. (In the Bernard-Golterman scalar ghost-quark formulation of quenched chiral perturbation theory [2], the negative sign of the scalar propagator arises from the dominance of a negative metric state consisting of a pair of ghost-quark mesons.)

II. LATTICE RESULTS FOR THE SCALAR PROPAGATOR

In a recent study of quenched chiral logs and the η' propagator [5], the MQA pole-shifting ansatz was applied to a set of quark propagators for an ensemble of 300 gauge configurations at $\beta = 5.7$ on a $12^3 \times 24$ lattice. The fermion action was clover-improved Wilson-Dirac with $C_{sw} = 1.57$. Nine values of quark mass were used, corresponding to a range of hopping parameters from $\kappa = .1400$ to .1428. Valence quark propagators were calculated from both local delta-function sources and from exponentially smeared sources in a Coulomb gauge. (For further details, see Ref. [5].) These pole-shifted quark propagators were used to calculate the scalar-meson propagators considered in this paper. The pion masses obtained from this ensemble have values ranging from $m_\pi a = 0.245$ to 0.603, and are listed in Table I.

It is natural to expect that the scalar $\bar{\psi}\psi$ correlator in QCD will be dominated by the coupling to the lightest scalar meson which is expected to have a mass larger than 1 GeV. For the heaviest-quark masses studied here, this is in fact the behavior observed for the quenched propagator. First, con-

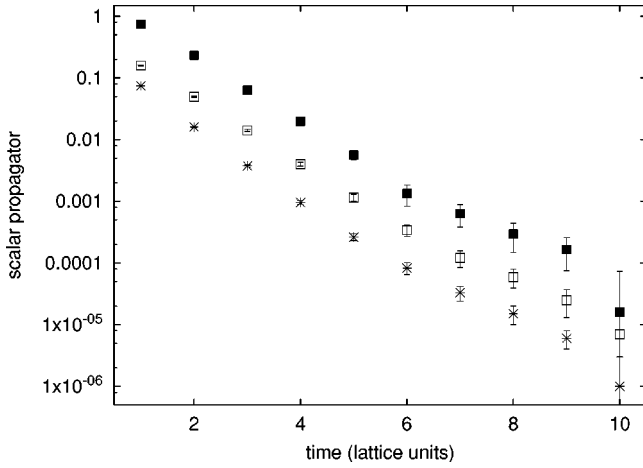


FIG. 3. The scalar propagator for the heaviest quark ($\kappa=.1400$) with local-local (*'s), smeared-local (empty boxes), and smeared-smeared (filled boxes) sources.

sider the scalar propagator for our heaviest-quark mass, with $m_\pi a = .603$, corresponding to $\kappa = .1400$. (From Ref. [5], we have $\kappa_c = 0.14329$ for clover-improved Wilson-Dirac fermions.) The measured values of the local-local, smeared-local, and smeared-smeared propagators are shown in the log plot in Fig. 3. As expected, the plot shows clear evidence of a massive scalar meson. For the smeared-local propagator, the time dependence is reasonably well described for $t > 2$ by an exponential fit with a mass of $M_s a = 1.25(2)$. The effective mass plot for the smeared-local propagator is shown in Fig. 4 for $\kappa = .1400$. For comparison, the effective mass for the local-local and smeared-smeared propagators is also plotted. Although the smearing function used (an exponential with exponent 0.5 in lattice units) was not tuned for this particular problem, it does a good job of removing excited-state contamination, giving a reasonably flat effective mass over several time slices from $t = 2$ to $t = 6$, and a nearly identical effective mass plot for smeared-local and smeared-smeared propagators (indicating an absence of excited states in both).

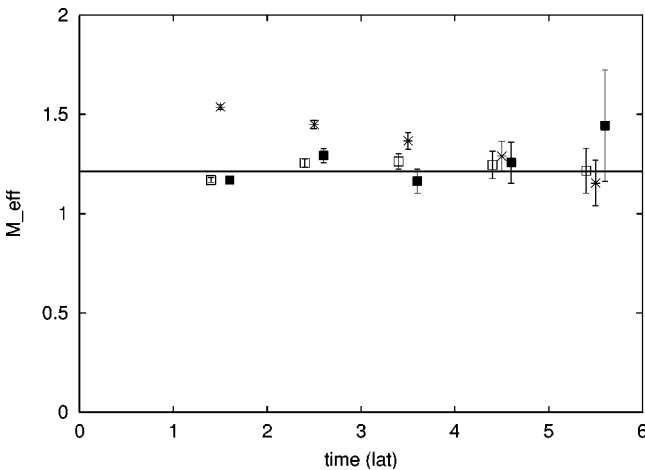


FIG. 4. Effective mass plot for $\kappa = .1400$ for local-local (*'s), smeared-local (empty boxes), and smeared-smeared (filled boxes) correlators.

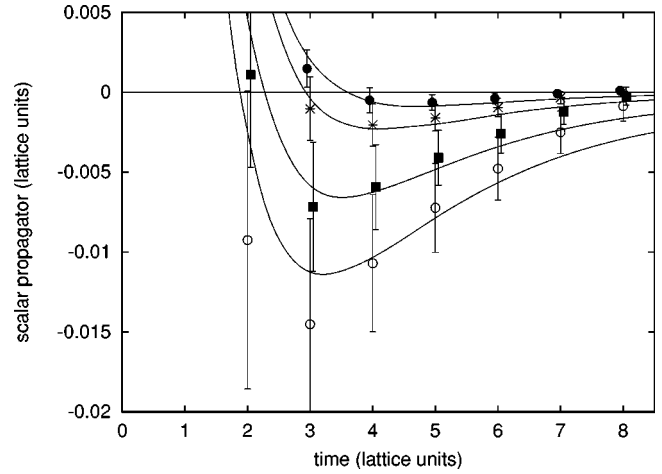


FIG. 5. Scalar propagator for $\kappa = .1423$ (filled circles), $.1425$ (*'s), $.1427$ (filled squares), and $.1428$ (open circles). Solid curves are fits to the bubble-sum formula, Eq. (19).

As pointed out in the Introduction, the behavior of the scalar propagator changes dramatically for the lighter-quark mass values. The results for the scalar propagator for our lightest-quark mass values are shown in Fig. 5, with $m_\pi a = .245, .267, .307, \text{ and } .342$, corresponding to κ values of $.1428, .1427, .1425, \text{ and } .1423$ respectively. Here we have plotted the local-local $\bar{\psi}\psi$ correlators. Instead of exhibiting the behavior expected for scalar-meson states, these propagators are dominated by a significant negative contribution in the range $t = 2$ to $t = 7$ which increases for lighter-quark masses. We interpret this behavior as a clear signal for the negative metric contribution associated with the $\eta' - \pi$ intermediate state discussed in the previous section.

The $\eta' - \pi$ loop interpretation of the anomalous component of the scalar propagator is made more convincing by noting that the leading chiral behavior of this contribution is entirely determined by current algebra in terms of parameters which have already been measured with this ensemble in our previous study of the pseudoscalar propagator [5]. The relevant chiral loop diagram is shown in Fig. 6, with the cross denoting the η' -hairpin mass insertion m_0^2 , and the open circles representing $\bar{\psi}\psi$ operator vertices. If we ignore form-factor effects at these vertices, we can calculate the $\eta' - \pi$ contribution to the $\bar{\psi}\psi$ propagator in momentum space. The propagator

$$\Delta(p) \equiv \sum_x e^{-ip \cdot x} \langle \bar{\psi}_1 \psi_2(x) \bar{\psi}_2 \psi_1(0) \rangle \quad (1)$$

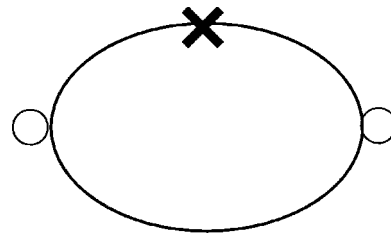


FIG. 6. One-loop quenched chiral perturbation theory graph evaluated in Eq. (2).

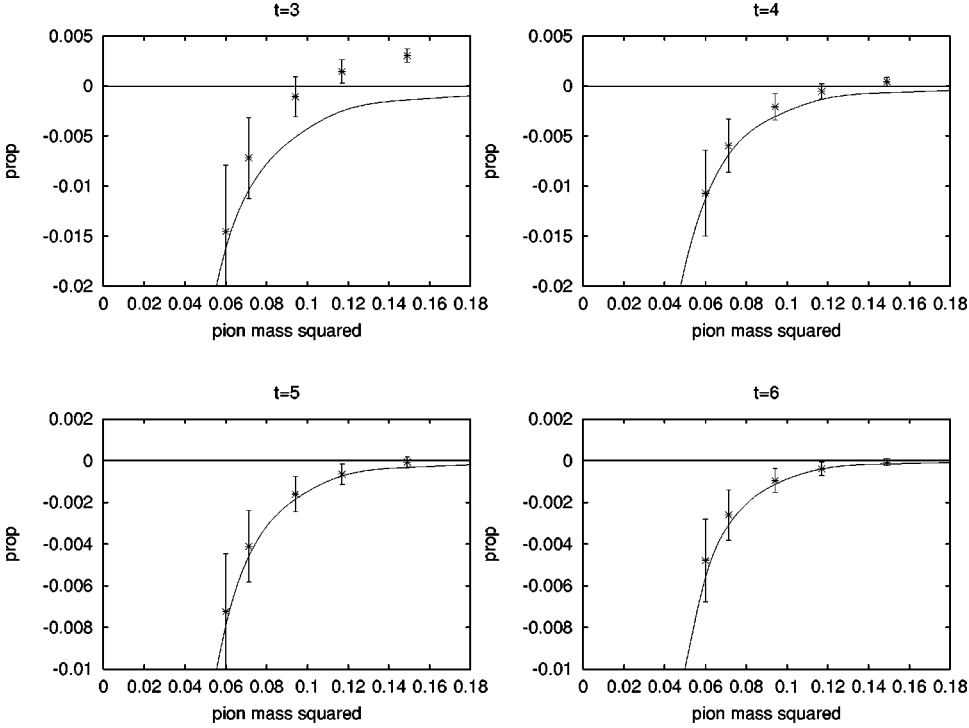


FIG. 7. Pion mass dependence of the scalar propagator for $t = 3, 4, 5, 6$.

is given in terms of the one-loop integral $B(p)$,

$$\Delta(p) \sim -C_B^2 B(p), \quad (2)$$

where

$$B(p) = \frac{1}{VT} \sum_k \frac{1}{[(k+p)^2 + m_\pi^2]} \frac{m_0^2}{(k^2 + m_\pi^2)^2}. \quad (3)$$

Here, C_B is the $\bar{\psi}\psi$ to η' - π coupling. (In the next section we will discuss including the scalar-meson intermediate state, along with form-factor/unitarization effects.) The pion mass values for the hopping parameters used here have already been reported in Ref. [5] and are listed here in Table I. The hairpin insertion mass m_0^2 is also determined in Ref. [5]. For clover-improved fermions with $C_{sw} = 1.57$ the value found in the chiral limit (dropping a flavor factor of $\sqrt{3}$ included in Table II of that reference) is

$$m_0 = .33(2). \quad (4)$$

The quark mass dependence of m_0 was found to be very mild (see Table II of Ref. [5]). Here, for simplicity, we will take it to be a mass independent constant given by Eq. (4). The only other parameter needed to evaluate the η' - π bubble contribution is the η' - π matrix element C_B of the scalar-density operator. In the quenched theory, this matrix element is related to the π - π matrix element of the isoscalar quark density using the soft-pion reduction of both matrix elements. This latter matrix element determines the m_π^2 vs m_q slope parameter, r_0 , in the chiral limit.

$$C_B = \sqrt{2} \langle 0 | \bar{\psi}_1 \psi_2 | \eta' \pi \rangle = \langle \pi^+ | \bar{\psi} \psi | \pi^+ \rangle = m_\pi^2 / m_q = 2r_0. \quad (5)$$

Note that the extra factor of $\sqrt{2}$ arises from the two flavor nature of the hairpin correlator. The slope parameter r_0 was determined by our fits to the pseudoscalar correlators in Ref. [5],

$$r_0 = 1.99(12). \quad (6)$$

Thus, in this approximation the effect of the η' - π bubble, Eq. (2), is completely predicted by chiral symmetry in terms of the constants (4) and (6), and the pion masses in Table I. The result for the lightest-quark mass ($\kappa = .1428$) is plotted along with the measured propagator in Fig. 1 (lower curve). Considering that the plotted curve has *no adjustable parameters*, it fits the size and shape of the propagator remarkably well in the time range from $t=3$ to $t=7$. For times $t < 3$, the measured propagator deviates from the one-loop expression in the positive direction, indicating that the spectral function also contains a heavy scalar meson. This short-range, positive metric exponential component dominates in the heavier-quark cases where the chiral loop effect becomes unimportant. The one-loop result also explains the pion mass dependence of the anomalous propagator component, as shown in Fig. 7, where we have plotted the value of the scalar propagator at various time separations as a function of m_π^2 . The solid curves are the p_0 Fourier transform at $\vec{p}=0$ of the one-bubble integral (2), with m_0 and r_0 given by Eqs. (4) and (6). Again the agreement with the data is surprisingly good, considering the absence of any adjustable parameters. The accurate description of both the time dependence and the pion mass dependence leaves little doubt that, for the lightest-quark masses, the scalar propagator over the range of times from about $t=3$ to 7 is completely dominated by the η' - π loop. Furthermore, this agreement shows that the soft pion theorem relating the scalar-density matrix element (5) to

the corresponding pseudoscalar matrix element is well satisfied by the lattice results. This is somewhat surprising at $\beta = 5.7$, where one might have expected substantial chiral symmetry violation from finite lattice-spacing effects.

For short time separations and/or heavier-quark masses, an accurate description of the scalar propagator requires positive contributions from scalar-meson states along with the negative η' - π component. In the next section, we present a derivation of the quenched scalar propagator based on a detailed chiral Lagrangian description which will be used to fit our data for all quark mass values. The corresponding propagator fits are discussed in Sec. IV.

III. QUENCHED CHIRAL PERTURBATION THEORY

According to the analysis of Bernard and Golterman, low-energy quenched QCD is described by an effective local field theory with degrees of freedom corresponding to meson bound-states, including not only ordinary $q\bar{q}$ mesons, but also $q'\bar{q}, q\bar{q}'$, and $q'\bar{q}'$ mesons, where q' is a wrong-statistics ghost quark. Order by order in the η' mass insertion m_0^2 , the ghost-quark formalism is easily seen to be equivalent to Sharpe's formulation, which begins with a $U(3) \times U(3)$ chiral Lagrangian combined with rules inferred from the structure of quark-line diagrams in the quenched theory. In this paper, as in our previous analysis [5], we follow the latter approach, invoking a chiral Lagrangian having a valence pion and η' degrees of freedom. To describe quenched QCD, the chiral Lagrangian is supplemented with rules which reflect the suppression of internal quark loops. As a result, all normal pion loops are suppressed except for cactus diagrams involving the η' meson connected by single insertions of the hairpin mass term. Using this procedure we obtained a consistent fit to our lattice data for the pseudoscalar valence and η' -hairpin propagators and determined the relevant chiral Lagrangian parameters. We now extend this analysis to the isovector, scalar propagator.

The appropriate effective field theory must now include a multiplet of scalar mesons in addition to the pion and η' degrees of freedom. Using standard chiral Lagrangian methods, the heavy scalar mesons are described by scalar fields transforming nonlinearly under chiral symmetry rotations. The resulting chiral Lagrangian is

$$\begin{aligned} \mathcal{L} = & \frac{f^2}{4} \text{tr}\{\partial U \partial U^\dagger\} + \frac{f^2}{4} \text{tr}\{\chi^\dagger U + U^\dagger \chi\} + \frac{1}{4} \text{tr}\{D\sigma D\sigma\} \\ & - \frac{1}{4} m_s^2 \text{tr}\{\sigma\sigma\} + g_s \text{tr}\{\sigma \sqrt{U} \partial U^\dagger \partial U \sqrt{U}^\dagger\} \\ & + f_s \text{tr}\{\chi^\dagger \sqrt{U} \sigma \sqrt{U} + \chi \sqrt{U}^\dagger \sigma \sqrt{U}^\dagger\} + \mathcal{L}_{\text{hairpin}}, \end{aligned} \quad (7)$$

where \mathcal{D} is a chiral covariant derivative, m_s the sigma mass, g_s the strength of the chiral invariant coupling of sigma mesons to pions, and f_s the strength of the corresponding chiral symmetry breaking interactions. Here we denote the scalar field by σ . (Elsewhere, when referring to particle states, we use the conventional a_0 and a_0^* to denote ground-state and

excited-state mesons.) The chiral field matrix U contains the pion and η' degrees of freedom. The η' mass term is given by the hairpin Lagrangian,

$$\mathcal{L}_{\text{hairpin}} = -\frac{1}{2} m_0^2 (f^2/8) [i \text{tr} \ln(U^\dagger) - i \text{tr} \ln(U)]^2. \quad (8)$$

We have not included interactions involving the couplings L_5 and L_8 used in our previous analysis of higher order terms in the sigma potential as they will have only small effects on our analysis of the isovector scalar propagator.

Scalar and pseudoscalar quark densities are represented by meson operators in the effective field theory and can be determined from the dependence of the chiral Lagrangian on the spurion field χ . Hence the isovector scalar-density operator is given by

$$\begin{aligned} \overline{\Psi}_2 \Psi_1 = & -\frac{1}{2} r_0 f^2 (U + U^\dagger)_{12} \\ & - 2r_0 f_s (\sqrt{U} \sigma \sqrt{U} + \sqrt{U}^\dagger \sigma \sqrt{U}^\dagger)_{12}; \end{aligned} \quad (9)$$

with

$$\chi = \chi^\dagger = m_\pi^2 = 2r_0 m_{\text{quark}}. \quad (10)$$

Our previous fits to the pseudoscalar propagator determined the following values for the chiral Lagrangian parameters,

$$\begin{aligned} f &= 0.1066(24), \\ m_o &= 0.33(2), \\ r_o &= 1.99(12). \end{aligned} \quad (11)$$

To lowest order, the local isovector scalar density may be expanded in terms of the pion, η' , and sigma fields,

$$\overline{\Psi}_2 \Psi_1 = \sqrt{2} r_0 (\pi^+ \eta') - 4 \sqrt{2} r_0 f_s (\sigma^+). \quad (12)$$

At tree level, only the sigma propagator gives a positive contribution to the scalar propagator

$$\langle \overline{\Psi}_2 \Psi_1 \quad \overline{\Psi}_1 \Psi_2 \rangle = 32 r_0^2 f_s^2 P_\sigma, \quad (13)$$

where P_σ is the a_0 meson propagator. The η' - π term can only contribute via a meson loop. However, the η' propagator in the loop is the η' -hairpin propagator with a single insertion of the hairpin mass, m_0^2 (see Fig. 2). Including only these terms, the scalar propagator is

$$\langle \overline{\Psi}_2 \Psi_1 \quad \overline{\Psi}_1 \Psi_2 \rangle = 32 r_0^2 f_s^2 P_\sigma + 4 r_0^2 B_{\text{hp}}. \quad (14)$$

In the last term above, an extra factor of 2 arises from the two flavor nature of the hairpin correlator. Here B_{hp} is the hairpin bubble:

$$B_{\text{hp}} = FT \left\{ \frac{1}{VT} \sum_k \frac{1}{[(k+p)^2 + m_\pi^2]} \frac{-m_0^2}{(k^2 + m_\pi^2)^2} \right\} \quad (15)$$

and FT means the Fourier transform on p . As discussed in the Introduction, the negative sign of the η' propagator in loops is dictated by the quenching and implies that this meson loop makes a negative contribution to the scalar propagator. It should also be noted that the η' propagator is more infrared singular than the normal valence pion propagator. This has a dramatic effect on the scalar propagator. In the light-quark limit, the quenched theory predicts that large negative chiral loop effects should dominate the scalar propagator. Our lattice data give convincing evidence for these effects.

A complete analysis of the scalar propagator must go beyond the lowest order terms given above. The chiral Lagrangian predicts couplings between the scalar meson and η' - π states as well as η' - π rescattering interactions generated by the symmetry breaking terms that give mass to the pion. These higher order terms involve η' - π bubble diagrams and can be resummed into a closed form. Since the chiral invariant interactions between the σ and η' - π states include derivative couplings, bubbles with derivative couplings at the $\sigma\eta'\pi$ vertex must, in principle, also be included. These terms are less infrared singular than the non-derivative terms and are not expected to play a major role in explaining the large quenched effects seen in the data. In the following analysis, we will neglect such derivative coupling terms. The formulas and results given below are for the equal quark mass case; generalizations to the unequal mass case are straightforward.

As is always the case in propagator studies, the presence of excited states in the spectral function complicates the analysis. As we discussed in Sec. II, in addition to the propagator for local $\bar{\psi}\psi$ operators, we have calculated propagators with a smeared source at one or both ends. In our previous analysis of the pseudoscalar channel [5], a full multistate fitting procedure was employed. Here we take a somewhat simpler approach which is suggested by features of the data. We model the spectral function in terms of three components: (1) the η' - π state, (2) a ground-state scalar meson a_0 , and (3) an excited-state scalar meson a_0^* . We perform an analysis of the local-local propagator by first using information from the smeared-local and smeared-smeared propagators to remove the excited-state a_0^* scalar-meson component and then fitting to a formula obtained by resumming all repeated bubble graphs involving the η' - π state and the ground-state a_0 scalar meson, as depicted in Fig. 8. To estimate and remove the contribution of the excited a_0^* from the local propagator, we consider first the case with the heaviest quark, $\kappa = .1400$. Within statistics, all of the scalar propagators for smeared and local sources exhibit the same time dependence beyond $t=3$. In fact, the smeared-local and smeared-smeared propagators are equal, up to an overall factor, at all time slices, as evidenced by the effective mass plot in Fig. 4. For the heavier-quark mass values, the η' - π loop is relatively unimportant, and the smeared and local propagators can be analyzed in terms of a ground-state and excited-state scalar meson. The fact that the smeared-local and smeared-smeared propagators $\Delta_{SL}(t)$ and $\Delta_{SS}(t)$ are proportional and that both give flat effective mass plots indi-

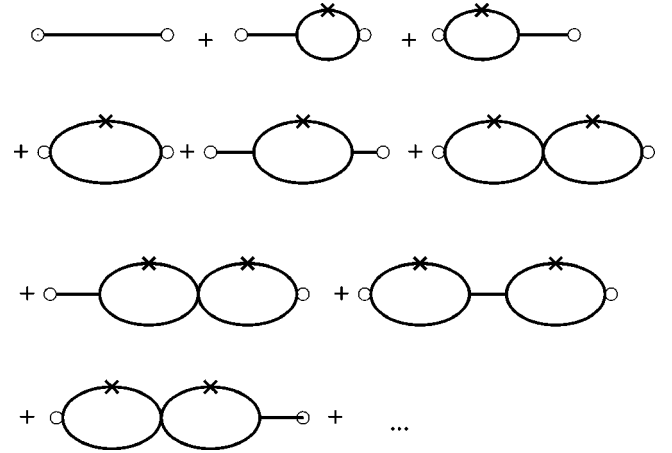


FIG. 8. Graphs which are included in the resummed scalar propagator, Eq. (19).

cates that neither propagator has a significant excited-state component. On the other hand, the local-local propagator clearly has a significant a_0^* component, as seen in the effective mass plot, Fig. 4.

It is straightforward to estimate the a_0^* contribution by using the (essentially time-independent) ratio Δ_{SL}/Δ_{SS} to determine the excited-state component of Δ_{LL} .

$$\Delta_{LL}(t) - \frac{\Delta_{SL}}{\Delta_{SS}} \Delta_{SL}(t) \sim C_{a_0^*} \exp(-m_{a_0^*} t). \quad (16)$$

Numerically, the above procedure applied to the $\kappa = .1400$ propagators gives excited-state parameters

$$C_{a_0^*} = 0.275(30), \quad m_{a_0^*} = 1.86(10). \quad (17)$$

The large mass obtained emphasizes that the excited-state contribution is only important at very short time separations. Similar results are obtained for $\kappa = .1405$ and $.1410$, with no significant observed dependence on quark mass. With this information, we can separate the excited-state component from the local-local propagator:

$$\Delta_{LL}(t) = C_{a_0^*} \exp(-m_{a_0^*} t) + \tilde{\Delta}_{LL}(t), \quad (18)$$

where $\tilde{\Delta}_{LL}(t)$ includes contributions from the η' - π state and from the ground-state scalar meson, and will be modeled by the bubble sum depicted in Fig. 8. For the lighter-quark masses, the η' - π state becomes important, and it is more difficult to disentangle the a_0 and a_0^* contributions. In the fits to the local-local propagator described in the next section, we have neglected the quark mass dependence of the excited-state a_0^* term and used the estimate (17) for all quark masses.

By resumming the multiple-bubble and scalar propagator graphs shown in Fig. 8, the full propagator may be written in terms of the one-loop bubble function $B(p)$ defined in Eq. (2),

$$\Delta(p) = -4r_0^2 B^{ren} + 32r_0^2 (f_s - f_s(2m_\pi^2/f^2) B^{ren}) \times (f_s - f_s(2m_\pi^2/f^2) B^{ren}) P_{a_0}, \quad (19)$$

where f_s is the coupling of the scalar meson to the $\bar{\psi}\psi$ density, $B^{ren}(p)$ is the resummed multiple-bubble function,

$$B^{ren} = \frac{B(p)}{1 + (2m_\pi^2/f^2)B}, \quad (20)$$

and P_{a_0} is the resummed a_0 propagator,

$$P_{a_0}^{-1} = \hat{p}^2 + m_s^2 + 32(f_s m_\pi^2/f^2)^2 B^{ren}. \quad (21)$$

Note that the negative sign associated with the hairpin insertion has been taken outside of the bubble function, i.e., the functions $B(p)$ and $B^{ren}(p)$ are both positive.

We use the bubble function $B(p)$ defined for the lattice version of the full chiral Lagrangian with the same lattice spacing as the quark lattice. In Eqs. (20),(21), the lattice four-momentum is defined by $\hat{p} \equiv 2 \sin(p/2)$ as appropriate for bosonic propagators. If we are to use the pion masses in Table I, which were determined from fitting the t -space pion propagators, then the pion masses used in lattice propagators above are given by $\tilde{m}_\pi = 2 \sinh(m_\pi/2)$.

This analysis includes all contributions to the scalar propagator which can be computed by direct η' - π bubble summation and mixing with the a_0 scalar-meson state. We use these expressions in our analysis of the lattice data on the isovector, scalar propagator.

The quenched theory does introduce additional contributions which could modify the behavior of the bubble terms. For example, pions can interact through double hairpin exchange diagrams whose infrared behavior is doubly enhanced. Therefore, virtual η' processes do not decouple in the infrared limit as is normally expected for soft-pion interactions but can generate long-range forces between mesons in the quenched theory. Preliminary estimates of these effects indicate they are negligible for the range of pion masses and lattice volume considered in this paper and they have not been included in our analysis.

IV. GLOBAL FITS AND DETERMINATION OF CHIRAL LAGRANGIAN PARAMETERS

In Sec. II we showed that the data for the scalar propagator for heavier-quark masses was dominated by the scalar-meson a_0 intermediate state (after removing the excited a_0^* contribution, as discussed in that section), while for light masses, it is dominated by the η' - π intermediate state. To get a consistent fit for all masses, we have found that the resummed formula (19) (Fig. 8) produces the most stable results. (The simpler alternative of using the sum of a scalar meson pole plus the single-bubble function gives fits with only slightly worse χ^2 's but the resulting fit parameters f_s and m_s are less stable as a function of quark mass.) All of the fits discussed in this section are based on the formula (19) with the parameters r_0 and f fixed at their previously determined values (11). We present the results of two different

TABLE II. Fit parameters for the scalar propagator, with m_s fixed to values shown. The fit range is $t=[1-6]$.

κ	m_s	f_s	m_0	χ^2/dof
.1400	1.200	.0568(12)	.336(22)	2.1/4
.1405	1.185	.0570(12)	.335(25)	2.3/4
.1410	1.170	.0571(13)	.335(27)	2.3/4
.1415	1.156	.0574(13)	.338(30)	2.1/4
.1420	1.142	.0575(14)	.346(33)	2.3/4
.1423	1.133	.0578(15)	.358(36)	3.0/4
.1425	1.128	.0576(16)	.360(43)	4.5/4
.1427	1.122	.0564(18)	.332(51)	6.4/4
.1428	1.119	.0555(20)	.298(64)	6.7/4

fitting procedures. In the first set of fits (Table I), we take the hairpin mass insertion parameter m_0 to be fixed at the value (11) and use the scalar propagator fits to extract the scalar-meson Lagrangian parameters f_s and m_s . In the second set of fits (Table II), we let m_0 be a fit parameter and investigate how well the scalar propagator data by itself determines the value of the hairpin insertion.

The fits which extract the scalar parameters, with m_0 held fixed, are given in Table I. We see that the value of the ground-state scalar mass parameter m_s is rather well determined for the heaviest-quark masses, but becomes less accurate for lighter masses, where the η' - π state dominates. A linear fit to the scalar mass values in Table I gives a value of

$$m_s = 1.14(7) \quad (22)$$

in the chiral limit. Using the charmonium scale $a^{-1} = 1.18$ GeV, this gives a scalar-meson mass of 1.34(9) GeV. The scalar decay constant f_s in the chiral limit is

$$f_s = .057(3). \quad (23)$$

In addition to extracting scalar parameters, it is interesting to carry out fits to the scalar propagator with m_0 as a fit parameter. This procedure emphasizes the fact that the scalar propagator data alone provides a fairly accurate estimate of m_0 which is independent of, and consistent with, the previous estimates in Ref. [5]. As we saw in the previous fits, the scalar mass m_s is well-determined for the heaviest quarks, but is poorly determined at the light-quark end. To obtain stable fits with m_0 as a fit parameter, we fix m_s to be given by a linear fit obtained from the three heaviest-quark values, $m_s = 1.106 + 1.145m_q$, where m_q is the bare quark mass $(\kappa^{-1} - \kappa_c^{-1})/2$ in lattice units. In this set of fits, f_s is found to be approximately independent of quark mass and is well approximated by Eq. (23) for all quark masses. The values of the η' mass parameter m_0 obtained from these fits are given in Table II and plotted in Fig. 9. A linear fit to this data gives

$$m_0 = 0.34(4) \quad (24)$$

in the chiral limit. This result, obtained from the scalar propagator data alone, is quite consistent with our previous

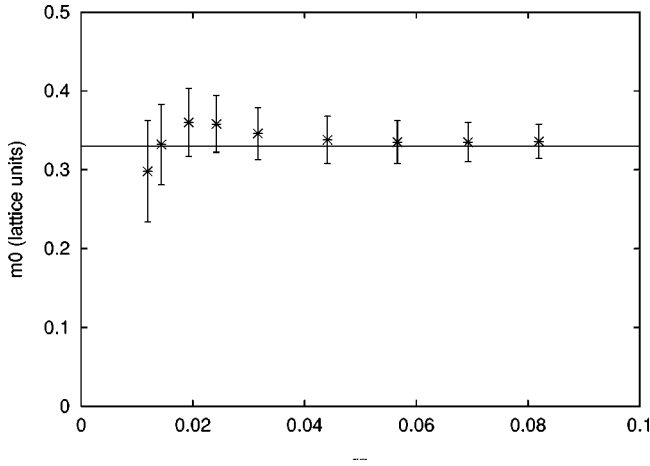


FIG. 9. Results for the η' -hairpin mass insertion extracted from fits to the scalar propagator. The solid line is the value obtained from direct analysis of the hairpin diagram in Ref. [5] (after removing a $\sqrt{3}$ flavor factor included in the definition of m_0 in that reference).

estimates which included direct η' -hairpin measurements, a topological susceptibility calculation, and QCL effects in the pseudoscalar channel [5].

One feature of the scalar propagator which appears to be somewhat inconsistent with our theoretical model is the behavior at larger time separations, $t \geq 7$. For the lightest quarks, we saw that the propagator was well described in the region $t=3$ to 6 by the one-loop η' - π bubble. However, beyond $t=6$, the propagator appears to go to zero (from below) more rapidly than the theoretical curve predicted by either the one-loop calculation or the bubble-sum formula, as shown for $\kappa = .1427$ in Fig. 10. If it is a significant departure from the chiral symmetry prediction, it could be an indication of strong η' - π interactions near threshold. Such interactions would normally be ruled out by soft-pion arguments, but may arise due either to explicit chiral symmetry breaking of the Wilson-Dirac action or because of higher order quenched effects. For the heaviest quarks, we also find that

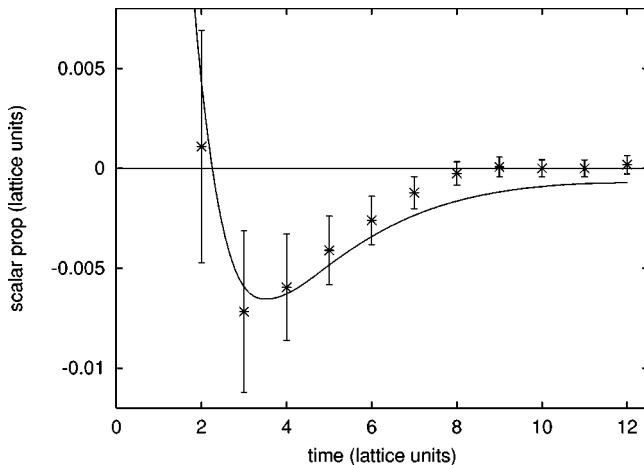


FIG. 10. Comparison of scalar propagator for $\kappa = .1427$ with the bubble-sum formula (19) fitted to the interval $t=1-6$.

the propagator appears to have an additional positive contribution for $t \geq 7$. For example, we can obtain a good fit (to both the heavy and light mass data at a large time) by adding a small π propagator term to the fit model. However, the origin of such a contribution is not presently understood within our model.

V. DISCUSSION

We have presented convincing evidence that the quenched scalar, isovector meson propagator exhibits a prominent “quenched chiral loop” (QCL) artifact at light-quark mass which is properly interpreted as the effect of an η' - π intermediate state. QCL effects that have been observed in other quantities [5,4] have been rather subtle, involving relatively small deviations from full QCD chiral behavior. By contrast, the QCL effect discussed here is an unmistakable chiral power singularity, and in fact dominates the scalar correlator for the lightest quark masses we have studied. The negative spectral weight of this contribution is a particularly vivid illustration of the oft-stated truism that the quenched approximation violates unitarity.

The results presented here also provide further evidence of the effectiveness of the pole-shifting ansatz of the modified quenched approximation. It is only after pole shifting that we are able to study the lightest-quark masses for which the η' - π state becomes obvious. It should be remarked, however, that even for the heavier-quark masses, the QCL effect is not negligible, and must be included in the fitting function in order to draw correct conclusions about the scalar-meson mass. For example, fitting the scalar propagator at the heavier-quark masses with a simple exponential and ignoring the η' - π contribution would lead to the erroneous conclusion that the scalar meson becomes *heavier* as the quark mass gets lighter. The resulting effect on the chiral extrapolation is at least as severe as typical QCL effects in the quenched light-hadron spectrum. For pion masses below about 400 MeV, the η' - π contribution becomes dominant, making the scalar-meson mass difficult to determine accurately. Nevertheless, by combining lattice calculations with quenched chiral perturbation theory, more extensive studies of scalar-meson spectroscopy in the quenched approximation should be feasible. Finally, the prominence of the QCL effect in the scalar valence propagator suggests that this propagator be added to the list of standard bellweather quantities (such as topological susceptibility, η' mass, and long-range static potential) which are expected to be particularly sensitive to the difference between quenched and full QCD gauge ensembles.

After completion of this work we learned of a paper by DeGrand who has also observed a negative isovector scalar correlator which he interprets as being due to zero modes of the Dirac operation [7]. In the context of the instanton liquid model [8] Schafer and Shuryak had made earlier observations of anomalous behavior of the isovector scalar propagator [9] using data from lattice calculations of Chu *et al.* [10]. We have no direct comments on the instanton liquid model analysis but prefer our interpretation in terms of quenched chiral loops.

ACKNOWLEDGMENTS

The work of W. Bardeen and E. Eichten was performed at the Fermi National Accelerator Laboratory, which is operated by University Research Association, Inc., under Contract No. DE-AC02-76CHO3000. The work of A. Duncan was supported in part by National Science Foundation Grant No.

PHY00-88946. The work of N. Isgur was supported by Department of Energy Contract No. DE-AC05-84ER40150 under which the Southeastern Universities Research Association (SURA) operates the Thomas Jefferson National Accelerator Facility (Jefferson Lab). The work of H. Thacker was supported in part by the Department of Energy under Grant No. DE-FG02-97ER41027.

-
- [1] S. Sharpe, Phys. Rev. D **46**, 3146 (1992).
[2] C. Bernard and M. Golterman, Phys. Rev. D **46**, 853 (1992).
[3] W. Bardeen, *et al.*, Nucl. Phys. B (Proc. Suppl.) **73A**, 243 (1999).
[4] S. Aoki *et al.*, Phys. Rev. Lett. **84**, 238 (2000); Nucl. Phys. B (Proc. Suppl.) **73**, 297 (1999).
[5] W. Bardeen, A. Duncan, E. Eichten, and H. Thacker, Phys. Rev. D **62**, 114505 (2000).
[6] W. Bardeen, A. Duncan, E. Eichten, G. Hockney, and H. Thacker, Phys. Rev. D **57**, 1633 (1998).
[7] T. DeGrand, Phys. Rev. D **64**, 094508 (2001).
[8] T. Schafer and E.V. Shuryak, Rev. Mod. Phys. **70**, 323 (1998).
[9] T. Schafer and E.V. Shuryak, Phys. Rev. D **54**, 1099 (1996).
[10] M.-C. Chu, J.M. Grandy, S. Huang, and J.W. Negele, Phys. Rev. D **48**, 3340 (1993).